

An efficient computational model for single-molecule optoelectronic devices

Original

An efficient computational model for single-molecule optoelectronic devices / Bottacin, Alberto; Mo, Fabrizio; Spano, Chiara Elfi; Ardesi, Yuri; Piccinini, Gianluca; Graziano, Mariagrazia. - In: JOURNAL OF COMPUTATIONAL ELECTRONICS. - ISSN 1569-8025. - 24:2(2025), pp. 1-13. [10.1007/s10825-025-02287-5]

Availability:

This version is available at: 11583/2997982 since: 2025-02-28T14:32:38Z

Publisher:

Springer

Published

DOI:10.1007/s10825-025-02287-5

Terms of use:

This article is made available under terms and conditions as specified in the corresponding bibliographic description in the repository

Publisher copyright

(Article begins on next page)



An efficient computational model for single-molecule optoelectronic devices

Alberto Bottacin^{1,3} · Fabrizio Mo¹ · Chiara Elfi Spano^{1,3} · Yuri Ardesi¹ · Gianluca Piccinini¹ · Mariagrazia Graziano²

Received: 9 September 2024 / Accepted: 2 February 2025
© The Author(s) 2025

Abstract

The growing interest in tuning the conduction properties of single-molecule junctions has drawn attention to studying their interaction with incident electromagnetic fields. The theoretical complexity of this problem necessitates the use of nonequilibrium statistical mechanics combined with quantum electrodynamics, leading to extremely time-consuming simulations. In this work, we propose a computationally efficient algorithm, which combines EE-BESD—an efficient and effective simulator of current–voltage characteristics in dark conditions—with approximated models for light interaction, specifically the Tien-Gordon and Floquet models. We validate EE-BESD-PAT through comparison with *ab initio* calculations and experimental data from the literature. Our computational model demonstrates good agreement with both experimental and density functional theory calculations, demonstrating that the proposed method is a promising computationally efficient tool without sacrificing accuracy.

Keywords Computational modeling · Molecular electronics · Photo-assisted tunneling · Single-molecule junctions · Optoelectronic devices · Tien-Gordon · Floquet

1 Introduction

In the last twenty years, systems such as molecular junctions have caught the attention of several research groups.

The reason is that molecules allow a further decrease in device dimensions, since they represent the ultimate limit of miniaturization, giving the possibility to discover and exploit new mechanical, electrical, optical and thermal phenomena at the nanoscale [1–8]. Since Aviram and Ratner’s pioneering concept of using single molecules as functional components in electronic devices [9], numerous proof-of-concept devices based on single-molecule junctions have been both theoretically demonstrated and experimentally developed. These developments have utilized various nanofabrication methods, including break-junction techniques, nanoetching and beam-induced deposition [10]. These molecular devices include a wide range of applications, such as molecular wires, switches, thermoelectric and optoelectronic devices, sensors, memory devices, nanoelectromechanical systems and transistors [11–25].

Generally, a combination of density functional theory (DFT) and nonequilibrium Green’s functions (NEGF) [26–29], implemented in commercial tools such as QuantumATK [30], is required for an accurate evaluation of the current–voltage (*I**V*) characteristic in single-molecule junctions in dark condition. However, the DFT+NEGF framework requires extended execution times that increase with the target accuracy. In previous works, our group developed an

✉ Alberto Bottacin
alberto.bottacin@polito.it

Fabrizio Mo
fabrizio.mo@polito.it

Chiara Elfi Spano
c.spano@inrim.it

Yuri Ardesi
yuri.ardesi@polito.it

Gianluca Piccinini
gianluca.piccinini@polito.it

Mariagrazia Graziano
mariagrazia.graziano@polito.it

¹ Department of Electronics and Telecommunications, Politecnico di Torino, Corso Duca degli Abruzzi, 24, Turin 10129, Italy

² Department of Applied Science and Technology, Politecnico di Torino, Corso Duca degli Abruzzi, 24, Turin 10129, Italy

³ Istituto Nazionale di Ricerca Metrologica, Strada delle Cacce, 91, Turin 10135, Italy

approximated method, called EE-BESD [31], which is based on an effective zero-dimensional (0D) model that allows computationally efficient estimation of IV curve. EE-BESD was conceived specifically to reduce extended execution times through approximations, allowing to efficiently compute the self-consistent field for any applied bias, while maintaining a good alignment with the *ab initio* model. This methodology enables the simulation of circuits composed of molecular junctions—an effort that becomes computationally infeasible when relying solely on the full DFT-NEGF framework.

In the recent past, the interest in the interaction of light with single-molecule junctions grew since it can be exploited to tune the conductive properties of molecular junctions through photo-assisted transport (PAT) [32–39] and trigger interesting physical phenomena, such as localized surface plasmons (LSPs), able to amplify the incident field [35, 40–42]. However, modeling this interaction for current-carrying molecular junctions is a challenging problem due to the complexity of the multi-body open systems under study [43, 44], which should be rigorously treated using nonequilibrium statistical mechanics combined with quantum electrodynamics. However, this approach dramatically increases the computational effort to predict the current flowing through the illuminated junction in stationary condition [30]. In the framework of NEGF, the self-consistent Born approximation (NEGF-SCBA) allows to define an additional self-energy, representing the interaction between electrons and photons, that should be computed self-consistently with the Green's functions [44–49]. NEGF-SCBA is extremely time-consuming and often a simplified version is implemented, as in QuantumATK where the self-consistent computation is truncated after the first iteration (first-order Born approximation) [30].

There exist two alternative models that are frequently applied to molecular junctions to describe the adiabatic photo-assisted transport, where it is assumed that no electronic excitations are happening in the molecule. The first is the one developed by P. K. Tien and J. P. Gordon in the field of superconductors [50, 51] and adapted to molecular junctions [52–55]. It is the most used model for PAT, even if its accuracy is low, because easier to apply and computationally efficient. The second model consists of the application of Floquet theory in the framework of NEGF. Indeed, assuming to study periodically driven systems, Floquet's theorem allows a great simplification of the time-dependent problem. This model has been extensively studied [56–65], but mainly applied to ideal molecular junctions described by a tight-binding approach and choosing electrical/optical parameters not strictly related to 'real' systems.

In this paper, we present a computational approach for the adiabatic photo-assisted transport analysis of realistic molecular junctions under stationary illumination conditions.

Under this assumption, we combined the aforementioned approximated models for the interaction of light with EE-BESD, with the aim to efficiently compute the conduction properties of the device, taking also into account possible plasmonic amplification. This approach, named EE-BESD-PAT, has been validated through the comparison with other simulations, obtained within the NEGF-SCBA framework, and with the experimental measurements by [66]. EE-BESD-PAT shows good agreement with both experimental and simulation results, confirming that the proposed method is advantageous in terms of execution time, reduced from days to minutes w.r.t. *ab initio* calculations without losing significant physical information. Furthermore, thanks to its computational efficiency, EE-BESD-PAT is suited to be included in photonic circuit-level simulators, thus opening the way to single-molecule optoelectronic devices and circuits.

2 Theoretical background

In this section, we briefly summarize how the charge transport in dark conditions is computed through EE-BESD. Then, we present the main approximated approaches used to model PAT through a single-molecule junction.

2.1 EE-BESD

EE-BESD is a 0D effective model used to analyze symmetric coupling molecular junctions, i.e., those for which the coupling molecule-source and molecule-drain are equal. The symmetry of the coupling does not limit the number of devices that can be studied. Indeed they are often obtained through mechanical break junctions, implying contacts made of the same material, with ideally the same crystallographic orientation and the same anchoring group.

Because of covalent bonds between the anchoring groups and the metallic contacts, this model is applied under the assumption of molecule-electrode strong coupling regime with associated coherent transport [29]. The electronic structure of the molecule is described by a finite number of energy levels (E_i), each of them characterized by a coupling coefficient γ_i . EE-BESD assumes a Lorentzian shape for energy level broadening, which is exact only if the contacts self-energy Σ^R is energy independent, with a different width depending on the level. Under this assumption and taking γ_i as the width of the i -th broadened level, the density of states (DOS) is expressed as:

$$DOS_i(E) = \frac{\frac{\gamma_i}{2\pi}}{(E - E_i)^2 + (\frac{\gamma_i}{2})^2} \quad (1)$$

where E corresponds to the energy value at which the density is computed. Considering the independent channel approximation, i.e., all levels conduct independently, it can be demonstrated that the transmission coefficient $T(E)$ can be expressed as [29]:

$$T(E) = \sum_{i \in \text{mol}} \pi \frac{\gamma_i}{2} D O S_i(E) = \sum_{i \in \text{mol}} T_i(E) \quad (2)$$

where T_i is the electron transmission probability through the i -th molecular channel/level.

In Eq. (2), $T(E)$ is independent on the applied bias (V_{DS}). Actually, when a static field is applied across the junction, the polarization of molecular orbitals and charging effects (transfer of electrons from molecule to contacts and vice versa) could change the intensity and position of the transmission peaks. To include these effects, a set of preliminary DFT-NEGF calculations are performed to extract information on the junction. Specifically, the IV characteristic and the corresponding transmission spectra are computed only for a reduced number of bias points in the desired range of V_{DS} (e.g., 11 points in [0, 3] V). From these results, it is possible to identify the position (E_i) of the most relevant transmission peaks and extrapolate their width (γ_i). Moreover, it is possible to evaluate the evolution with V_{DS} of each peak intensity by recurring to a second-order polynomial fitting, identified with $w_i(V_{DS})$. This procedure is beneficial since allows to extrapolate accurate parameters computed with ab initio calculations, which are done only once and for a low number of bias points.

Knowing the evolution of the peaks with V_{DS} allows to change the transmission spectrum by multiplying each coefficient $T_i(E)$, related to i -th level, with the corresponding polynomial fitting:

$$T(E, V_{DS}) = \sum_{i \in \text{mol}} T_i(E) w_i(V_{DS}) \quad (3)$$

Regarding charging effects, a self-consistent field (SCF) approach is employed to compute the potential variation U_{SCF} , which is responsible for a rigid shift in the energy of the transmission spectrum. The self-consistent loop is over the variable U_{SCF} , which is used to test convergence within the target tolerance [31].

Eventually, the current is computed through the Landauer–Büttiker formula using the transmission spectrum which takes into account polarization and charging effects [29] for any applied bias within the considered range of voltage values:

$$I(V_{DS}) = \frac{2e}{h} \int_{-\infty}^{+\infty} T(E, V_{DS}) [f_S(E) - f_D(E)] dE \quad (4)$$

where the constants e and h correspond to the elementary charge and the Planck constant, while the Fermi–Dirac distribution inside the contacts are identified by $f_S(E) = f(E, E_{F_S})$ for the source (S) and $f_D(E) = f(E, E_{F_D})$ for the drain (D), where $E_{F_{D/S}}$ represents the quasi-Fermi level inside the contacts.

2.2 Modeling light interaction

In the past years, approximated models have been proposed to evaluate the current resulting from adiabatic PAT across a molecule. To simplify the treatment, we neglect the effects associated with the magnetic field and other second-order effects (thermal expansion, hot electrons generation and thermo-electricity). Moreover, we consider a monochromatic electric field described in the classical form:

$$\mathbf{E}(t) = \mathbf{E}_{\text{inc}} \cos(\omega t) \quad (5)$$

where E_{inc} is the amplitude at junction site, and ω is the pulsation of the electric field.

The idea behind this approach is the following: If light polarization is mostly parallel to the transport direction, an oscillating potential $V_{AC}(t)$ drops between the contacts and the molecule inducing a classical modulation of the potentials. The result is a time-dependent current (AC contribution), but also an additional DC component, i.e., the photocurrent, which is modeled by Tien-Gordon and Floquet models. To ensure that the type of transport through the molecule is adiabatic, the radiation frequency ω should be smaller than the plasma frequency ω_p of the contacts in order to neglect the creation of electron–hole pairs. Moreover, to guarantee that the potential is uniform across the molecule, the radiation wavelength λ should be longer than d_{gap} , which represents the distance between the atomic contacts (it is approximately the length of the molecule) [56].

[58] proved a closed-form equation for the evaluation of the total steady-state current considering a classical monochromatic electromagnetic field. It is valid only when considering electron–electron interaction, inside the molecule, in a self-consistent way (as done in EE-BESD) and assuming an energy-independent density of states in the contacts, i.e., the so-called wide-band limit (WBL). The equation assumes the following Landauer-like form:

$$I(V_{DS}, V_{AC}) = \frac{2e}{h} \sum_{n=-\infty}^{\infty} \int_{-\infty}^{+\infty} [T_{DS}^{(n)}(E, V_{DS}, V_{AC}) f_S(E) - T_{SD}^{(n)}(E, V_{DS}, V_{AC}) f_D(E)] dE \quad (6)$$

In Eq. (6), two transmission spectra, $T_{DS}^{(n)}$ and $T_{SD}^{(n)}$, are defined to describe charge transport from source to drain and vice

versa. The number of exchanged energy quanta $\hbar\omega$ between electrons and the incident field corresponds to $|n|$, where n identifies the order of the transmission mode: absorption events are represented by $n > 0$, whereas $n < 0$ refers to emission processes. These mechanisms are weighted by the integral over energy and then summed together in order to evaluate the total current.

It can be proved that in general $T_{DS}^{(n)} \neq T_{SD}^{(n)}$ due to an external periodic driving force such as the one induced by an incident electric field [58]. Nevertheless, when a molecular junction is characterized by generalized parity, as in the case of symmetric junctions analyzed in EE-BESD, we have that $T_{DS}^{(n)} = T_{SD}^{(n)} \equiv T^{(n)}$ [58], where $T^{(n)}$ can be computed by Tien-Gordon and Floquet models. In the following, we will summarize these models, showing how they can be used to compute $T^{(n)}(E, V_{DS}, V_{AC})$.

2.2.1 Tien-Gordon model

The central idea in Tien-Gordon (TG) model is that the induced potential $V_{AC}(t)$ modulates over time the occupation of the electron energy levels in the contacts while maintaining the same carrier distribution across the levels of the molecule [50].

Considering an optically-induced oscillating potential that drops symmetrically at the two contacts and it is uniform along the molecule, it is possible to demonstrate that the transmission spectrum referred to n exchanged energy quanta is [54] (for simplicity of notation we do not report the dependence on V_{DS} and V_{AC}):

$$T^{(n)}(E) = J_n^2\left(\frac{\alpha}{2}\right)T(E + n\hbar\omega) \quad (7)$$

where $\alpha = \hbar\omega/eV_{AC}$ is an adimensional parameter related to the incident radiation strength; J_n is the Bessel function of the first kind of n -th order, and $T(E + n\hbar\omega)$ is the transmission spectrum in dark condition shifted by $n\hbar\omega$.

The main advantage of the Tien-Gordon model is that PAT can be computed starting from the properties of the junction in dark conditions. This scheme is numerically efficient and straightforward to be implemented. The main practical issue is that V_{AC} is not generally known and is considered as a varying parameter to fit the measurements in several experimental papers [39, 66]. In this work, we estimate its value starting from the parameters of the incident radiation, as it will be shown in Sect. 3.

2.2.2 Floquet model

The Floquet model represents the natural approach to deal with periodically light-driven molecular junctions since it exploits the time periodicity of the Hamiltonian. In the case

of incident monochromatic fields, we assume that the induced oscillating potential $V_{AC}(t)$ affects the energy levels of the molecule, expressed in the molecular Hamiltonian $H_{mol}(t)$, as follows [60]:

$$H_{mol}(t) = H_{mol,0} - eV_{AC}(t) \quad (8)$$

where $H_{mol,0}$ is the Hamiltonian of the molecule before the light interaction, whereas $-eV_{AC}(t)$ is the oscillating potential energy induced by the electric field. The latter term is responsible for the time periodicity of the Hamiltonian, which satisfies the relation $H_{mol}(t + \phi) = H_{mol}(t)$, with $\phi = 2\pi/\omega$. It can be proved that this time dependence is also inherited by the Green's functions of the system and it can be exploited to decompose the two times retarded Green's function, $G^R(t, t')$, in the following way [60, 65]:

$$G^R(t, t') = \sum_{n=-\infty}^{+\infty} \int_{-\infty}^{+\infty} \frac{1}{2\pi} G^{R(n)}(E) e^{-\frac{i}{\hbar}E(t-t') + in\omega t} dE \quad (9)$$

The functions $G^{R(n)}$ are called retarded Floquet modes and are related to photo-assisted mechanisms which involve the interaction with $|n|$ photons. They allow moving from the time domain to the energy domain, which is crucial since it simplifies the description of the system, as it is normally done in steady-state conditions.

The computational complexity of this approach is hidden in the Floquet modes. There are different schemes for their evaluation, which always involve inversion of matrices [63], corresponding to the time-consuming part of the algorithm. In this paper, we decided to follow the procedure described by [60], where a matrix continued fraction approach [59] is used to recursively solve the well-known Floquet-Dyson's equation of the Green's function formalism.

Knowing the Floquet modes, it is possible to compute the transmission coefficients under illumination condition [60]:

$$T^{(n)}(E) = \text{Tr}[\Gamma(E)G^{A(n)}(E + n\hbar\omega)\Gamma(E - n\hbar\omega)G^{R(n)}(E + n\hbar\omega)] \quad (10)$$

where $G^{A(n)}(E)$ is the advanced Floquet mode, calculated from the retarded component ($G^{A(n)}(E) = [G^{R(n)}(E)]^\dagger$), and $\Gamma(E)$ is the broadening function which results from the interaction between the molecule and one of the two reservoirs. Since we considered only symmetric molecular junctions, the broadening function related to source and drain coincides: $\Gamma_S = \Gamma_D \equiv \Gamma$.

3 Implementation

In this section, we show our algorithm implementation of Tien-Gordon and Floquet models, which is called EE-BESD-PAT, written in MATLAB. Our choice of starting from EE-BESD for the implementation has been driven by the need for computational efficiency and acceptable accuracy.

3.1 EE-BESD-NEGF

Firstly, we rewrite the EE-BESD suite in the Green's function formalism, since the Floquet model and the scheme described by [60] are both based on such a formal framework. Accordingly, we converted the arrays of energy levels and coupling factors into matrices in order to compute Green's functions. In particular, considering a molecular system with N energy levels, the Hamiltonian of the molecule can be expressed in the well-known diagonalized form:

$$H_{mol,0} = \begin{bmatrix} E_1 & & & \\ & E_2 & & \\ & & \ddots & \\ & & & E_N \end{bmatrix} \quad (11)$$

where the diagonal entries correspond to the energy levels of the molecule. Similarly, it is possible to express the broadening function through the coupling coefficients γ_i (already mentioned in Sect. 2) as follows:

$$\Gamma = \begin{bmatrix} \gamma_1 & & & \\ & \gamma_2 & & \\ & & \ddots & \\ & & & \gamma_N \end{bmatrix} \quad (12)$$

Assuming WBL, we know that the retarded contacts' self-energy, that is the contribution to the electron's energy due to the interaction with the contacts, is expressed by $\Sigma^R = -\frac{i}{2}\Gamma$, therefore, the retarded Green's function is computed through Dyson's equation:

$$G^R(E) = [EI - H_{mol,0} - \Sigma^R]^{-1} \quad (13)$$

where I is the identity matrix and the product EI corresponds to a diagonal matrix whose entries are all equal to the energy value E . It is known that, varying the applied bias, the nonequilibrium Green's function would change due to a variation of the coupling with the contacts. Nevertheless, assuming WBL and using Eq. (12), Σ^R remains the same for any applied bias. This approximation would lead to a wrong evaluation of the IV characteristic with respect to ab initio simulations. In order to include the dependence from V_{DS} ,

we rethought what is done in EE-BESD and adapted the fitting procedure to the NEGF algorithm. We defined a new energy-dependent fitting coefficient:

$$w_{NEGF}(E, V_{DS}) = \frac{\sum_{i \in mol} T_i(E) w_i(V_{DS})}{\sum_{i \in mol} T_i(E)} \quad (14)$$

This coefficient is used to compute Green's functions through a new definition that allows to include the bias dependence:

$$G^{R/A}(E, V_{DS}) = \sqrt{w_{NEGF}(E, V_{DS})} G^{R/A}(E) \quad (15)$$

with G^R coming from Eq. (13) and $G^A = [G^R]^\dagger$. To justify this definition, it is enough to compute the transmission spectrum for steady-state conditions:

$$\begin{aligned} T(E, V_{DS}) &= \text{Tr}[\Gamma_S \sqrt{w_{NEGF}(E, V_{DS})} G^R(E) \\ &\quad \Gamma_D \sqrt{w_{NEGF}(E, V_{DS})} G^A(E)] \\ &= w_{NEGF}(E, V_{DS}) \\ &\quad \text{Tr}[\Gamma_S G^R(E) \Gamma_D G^A(E)] \\ &= \frac{\sum_{i \in mol} T_i(E) w_i(V_{DS})}{\sum_{i \in mol} T_i(E)} \cdot \sum_{i \in mol} T_i(E) \\ &= \sum_{i \in mol} T_i(E) w_i(V_{DS}) \end{aligned} \quad (16)$$

The last line in Eq. (16) corresponds to the transmission spectrum computed with the original EE-BESD algorithm, thus the definition in Eq. (15) leads to the same result and allows to obtain the Green's functions depending on bias. This reformulation of EE-BESD in the context of NEGF is suitable for the implementation of Stefanucci et al.'s algorithm, which has been used to compute the Floquet modes as stated above.

3.2 EE-BESD-PAT

The first step toward the implementation of EE-BESD-PAT is to define the evaluation of V_{AC} , which is the main parameter Tien-Gordon and Floquet models are based on. In our algorithm, we consider the photon flux (F_{ph}) and the photon energy (E_{ph}) of the incident radiation as the main input parameters. From these quantities, we estimate the amplitude V_{AC} through classical electromagnetism: knowing F_{ph} and E_{ph} , the incident power density per unit area is expressed by $P_\Sigma = F_{ph} E_{ph}$; it is also known that the active power density carried by plane waves is related to the electric field as follows:

$$P_\Sigma = \frac{1}{2} \Re\{Y\} E_{inc}^2 \quad (17)$$

where Y is the characteristic admittance of the medium through which the radiation propagates. Considering the case

of vacuum (or air), $Y = \sqrt{\epsilon_0/\mu_0} = \epsilon_0 c$, and inverting Eq. (17), we retrieve the magnitude of the electric field:

$$E_{inc} = \sqrt{\frac{2F_{ph}E_{ph}}{\epsilon_0 c}} \tag{18}$$

Assuming a uniform drop of the potential along the single-molecule channel, we estimate V_{AC} as:

$$V_{AC} = E_{inc} d_{gap} k_{enh} \tag{19}$$

where k_{enh} is an amplification parameter that takes into account possible near-field enhancement caused by triggered LSP in the atomic contacts. This procedure is coherent with what is seen in the literature [36], permitting to analytically approximate V_{AC} . In EE-BESD-PAT, the value of k_{enh} is chosen by the user and becomes one of the input optical parameters.

As already stated in Sect. 2.2, it is possible to compute the current under illumination condition through Eq. (6), which is the figure of merit we want to evaluate with EE-BESD-PAT. Since only symmetrical junctions are considered, we define an overall ‘optical’ transmission spectrum that ideally takes into account all possible photo-assisted mechanisms, and it is used to compute the steady-state current:

$$T_{opt}(E) = \sum_{n=-\infty}^{\infty} T^{(n)}(E) \tag{20}$$

$$I(V_{DS}, V_{AC}) = \frac{2e}{h} \int_{-\infty}^{+\infty} T_{opt}(E) [f_S(E) - f_D(E)] dE \tag{21}$$

$T_{opt}(E)$ and $I(V_{DS}, V_{AC})$ represent the two main outputs of EE-BESD-PAT algorithm. The summation over n in Eq. (20) is truncated to a maximum order $\pm n_{max}$, that is chosen by the user and must be great enough to ensure convergence of the transmission spectrum.

The EE-BESD-PAT algorithm is shown in Fig. 1 through a block diagram. EE-BESD is still the first step of the algorithm, and it is used to compute the self-consistent potential U_{SCF} and the transmission spectrum in dark conditions (labeled T_{dark} to avoid confusion). From this point, the algorithm is divided into two branches, one for each PAT model. The Floquet branch starts from the evaluation of w_{NEGF} , $H_{mol,0}$ and Σ^R ; then follows the recursive solution of Floquet-Dyson’s equation (for each value of energy E) whose solutions are the Floquet modes used to calculate T_{opt} ; eventually, the current under illumination condition is computed. On the other hand, the Tien-Gordon branch is much shorter: it involves only shifts of the transmission spectrum in dark conditions and evaluation of the Bessel’s functions. After this step, it is possible to evaluate T_{opt} and then the

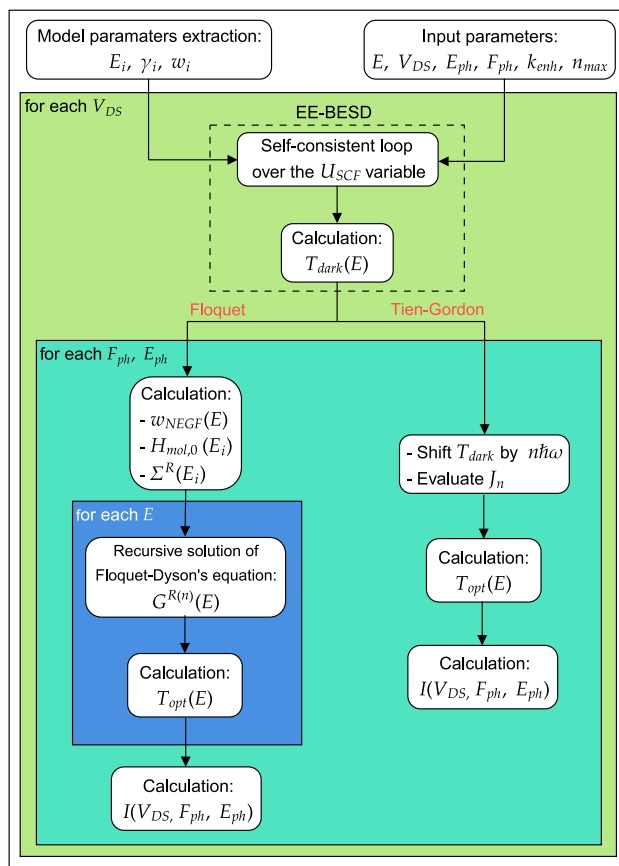


Fig. 1 Block diagram of EE-BESD-PAT algorithm. It is divided into two main phases: the first corresponding to the original EE-BESD algorithm (dashed rectangle) and the second represented by the computation of T_{opt} and $I(V_{DS}, F_{ph}, E_{ph})$ through Floquet and Tien-Gordon models (two branches starting from EE-BESD block). The filled rectangles in the diagram represent different cycles, whose iteration variables are indicated on the top-left corners

overall current. The whole algorithm must be repeated for each V_{DS} , whereas the two branches should be iterated for each combination of F_{ph} and E_{ph} . Indeed, in the block diagram, the filled rectangles represent different cycles, whose iteration variables are indicated on the top-left corners.

EE-BESD-PAT allows to compute figures of merit (T_{opt} and I) in short execution times, while preserving the essential physics behind PAT. In the following section, we present the results obtained with this simulator, especially focusing on its validation through comparison with ab initio simulations and experimental results.

4 Results and validation

To show the potentiality of our simulator, we reported the computed current in dark and in illumination conditions for three different dithiolated molecules (already included in the EE-BESD library) placed between two gold contacts:

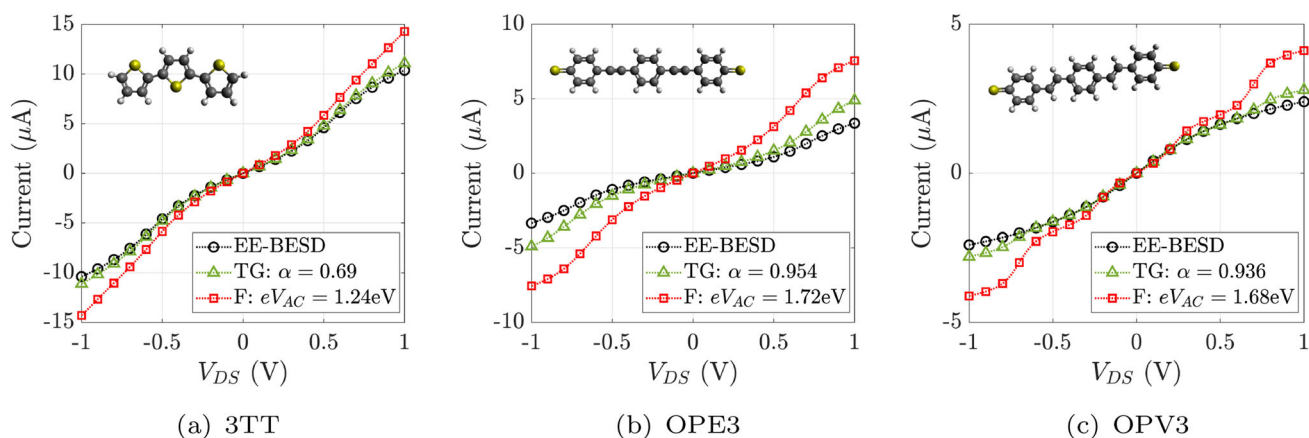


Fig. 2 *IV* characteristics of 3TT, OPE3 and OPV3 under dark (black circles) and illumination conditions (red squares and green triangles). Photons impinge on the single-molecule junctions with energy $E_{ph} = 1.8 \text{ eV}$ and flux $F_{ph} = 1 \times 10^8 \text{ s}^{-1} \text{ \AA}^{-2}$

terthiophene (3TT), oligophenylene ethynylene (OPE3) and oligophenylene vinylene (OPV3).

The corresponding *IV* characteristics, shown in Fig. 2, have been computed for the range $V_{DS} \in [-1, 1] \text{ V}$ considering an incident flux equal to $1 \times 10^8 \text{ s}^{-1} \text{ \AA}^{-2}$ and a photon energy of 1.8 eV ($\approx 689 \text{ nm}$), which is suited for LSP excitation. To include such effect, we arbitrarily posed $k_{enh} = 500$, coherent with field amplifications seen between gold nanoparticles [67], which has the effect to enhance the electric field in the gap, and as a consequence, to increase the value of V_{AC} . Finally, we considered for both models $n_{max} = 18$ (37 orders). Figure 2 reports in black with circular markers the *IV* curves in dark conditions computed with EE-BESD, which are symmetrical with respect to the origin, which it is expected in symmetric single-molecule junctions where source and drain are equivalent. Red squares and green triangles are the markers of the curves computed employing our proposed implementation of Floquet and Tien-Gordon models, respectively. Both of them predict an enhancement of the current through photo-assisted mechanisms, with Floquet evaluating a larger additional photocurrent than Tien-Gordon. This difference is traceable to different predicted heights of the sidebands generated by absorption or emission of energy quanta.

An example of illuminated transmission spectrum (T_{opt}) is reported in Fig. 3 for OPV3 considering a bias of 0.8 V . Solid black lines indicate the main peaks computed with EE-BESD in dark conditions, whereas in dashed red and dotted green, we see the transmission spectra evaluated with Floquet and Tien-Gordon. The additional peaks are distant $n\hbar\omega$ from the main peaks, whose transmission probability decreases due to light interaction. In other words, the effect of the impinging radiation is to excite the formation of transmission sidebands through which the electrons are transmitted from S to D electrodes. Because of mass conservation, each excited electron contributes to transmission at a different energy E (multiple

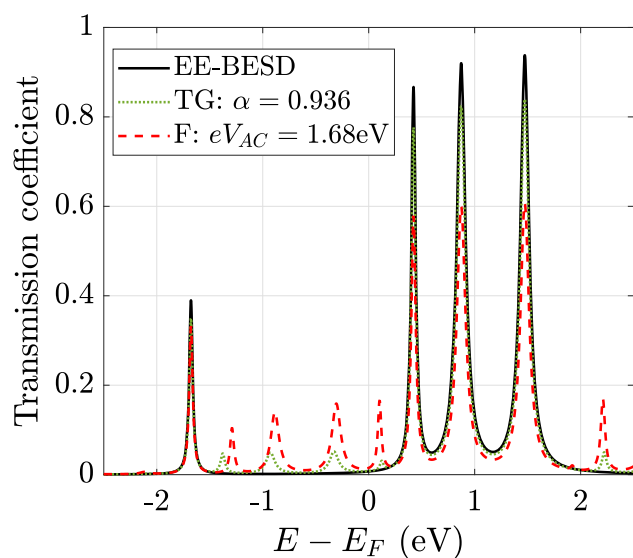


Fig. 3 Transmission spectrum of OPV3 under dark (solid black curve) and illumination conditions (dashed red and dotted green curves) at $V_{DS} = 0.8 \text{ V}$

or submultiple of $\hbar\omega$) w.r.t. its initial energy, thus creating a transmission path at that specific energy while decreasing the transmission probability at initial energy E . This mechanism, which is still perfectly caught within the developed EE-BESD-PAT, is at the basis of the electron transmission feature modulation by incident light, and thus at the origin of the photocurrent.

4.1 QuantumATK and EE-BESD-PAT comparison

We validate EE-BESD-PAT through a comparison with ab initio simulations employing QuantumATK and a comparison with an experiment. Starting from the first, we consider a 3TT single-molecule junction (depicted in Fig. 4) having

Fig. 4 3TT single-molecule junction considered for comparison between QuantumATK and EE-BESD-PAT. The image has been produced using the builder tool of QuantumATK

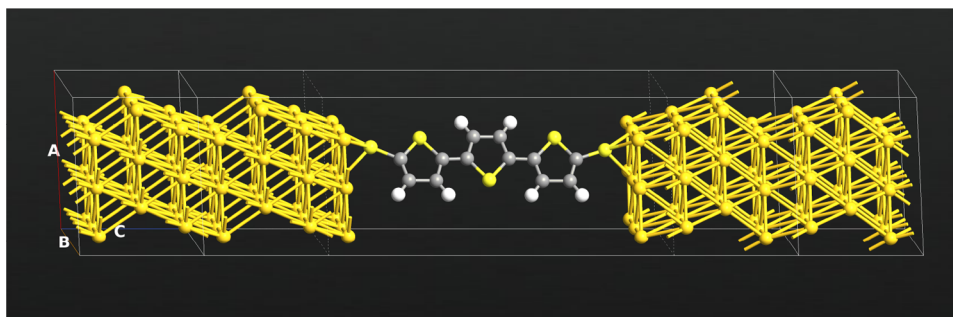


Table 1 Parameters for LCAO calculator and transport analysis through DFT-NEGF algorithm

Parameter	Value
Functional	GGA-PBE
Basis set	FHI-DZP
LCAO k-points	Preset density [4.0, 4.0, 150.0] Å
Poisson solver	Parallel conjugate gradient
Boundary conditions	A: Periodic, B: Periodic, C: Dirichlet
V_{DS}	[0, 3] V, 11 points
Electron energy	[-2.5, 2.5] eV, 151 points
DFT-NEGF k-grid	Densities along A and B: [7.0, 7.0] Å

gold electrodes with orientation [1,1,1]. With QuantumATK, we compute the photocurrent using first-order Born approximation in the NEGF framework. QuantumATK is only able to compute the photocurrent for different photon energies but at a specific bias point. To choose the most appropriate V_{DS} , we made a preliminary study of the IV characteristic. For the computation of the electronic structure and the analysis of transport, we used the parameters shown in Table 1. After looking at the results and extracting the parameters for the EE-BESD implementation, we decided to choose $V_{DS} = 0.3$ V as bias point since the transmission spectrum obtained with EE-BESD overlaps well with the one retrieved with QuantumATK for energies near the Fermi level (see Fig. 5). In this way, we have the best comparison since we exclude unmatched shifts of the spectrum, due to pronounced charging effects, and reduce the differences owing to the limited number of molecule levels that EE-BESD-PAT considers.

With this in mind, we computed the photocurrent setting the parameters as shown in Table 2 and compared the result with EE-BESD-PAT simulation. The QuantumATK simulation required 5 days to finish. On the other hand, the EE-BESD-PAT simulation took 7 min setting $n_{max} = 18$ and considering 125 photon energy points. The time needed for the EE-BESD parameterization is not included in the 7 min since only the time for photocurrent computation is compared. Nevertheless, for the considered molecule and applied

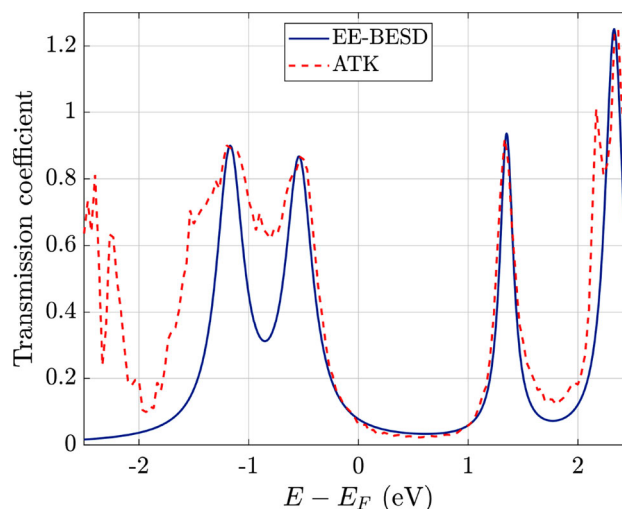


Fig. 5 Transmission spectrum of 3TT at $V_{DS} = 0.3$ V obtained with EE-BESD and QuantumATK

Table 2 Parameters set for ab initio photocurrent evaluation of 3TT junction at $V_{DS} = 0.3$ V

Parameter	Value
Electron energy	[-2.7, 2.7] eV, 99 points
Photon energy	[0, 2.5] eV, 20 points
k-points grid	MonkhorstPackGrid 15 × 15
Polarization	Linear-z [0,0,1]

bias, an automatic fitting procedure can be applied and a good-quality fit is obtained in a short time. Even in the case of a manual fit, less than an hour of work is sufficient for retrieving a good fit of the transmission spectrum.

Although we set a low number of photon energies (20 points), the simulation performed in QuantumATK requires execution times that are far longer than those needed by EE-BESD-PAT, proving the high efficiency of our computational scheme.

Figure 6 shows the results of this comparison. First of all, this is important to observe the order of magnitude of the photocurrent: it is the same for each model and equal to 10^{-19} A.

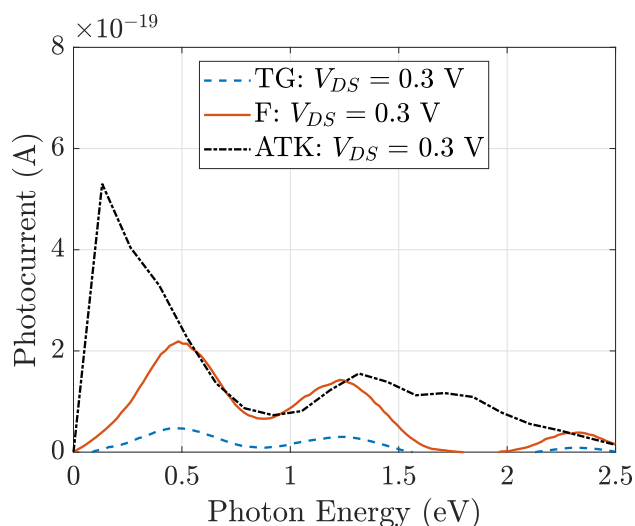


Fig. 6 Photocurrent of 3TT at $V_{DS} = 0.3$ V computed through EE-BESD-PAT and QuantumATK. The incident photon energy is varied, while the flux remains fixed to $F_{ph} = 1 \times 10^8 \text{s}^{-1} \text{\AA}^{-2}$

This value is not strange if we focus on the chosen photon flux. Indeed, only one photon per second reaches an area of 1\AA^2 , where can interact with one electron in an energy state outside the bias window. The interaction can lead the electron to move in a molecular orbital involved in conduction, hence increasing the total current. Considering typical dimensions of a single-molecule junction, only a few photons per second can interact with a corresponding number of electrons; therefore, the additional charge involved in conduction is a small multiple of the elementary charge, which is proportional to 10^{-19}C .

For what concerns the general behavior, the photocurrent obtained with QuantumATK shows a peak at $E_{ph} \approx 1.3$ eV and another close to small values of photon energy. The first peak is related to a local maximum of available states that can accept electrons after having absorbed or emitted an energy quanta. The result is a peak in the photocurrent. On the other hand, the peak close to 0 eV should be considered with attention since its intensity could strongly depend on the number of photon energies and the considered number of k-points. Moreover, due to the computational complexity and the order of magnitude of the photocurrent, numerical errors in ATK could not be completely neglected.

A similar shape of the photocurrent results from Tien-Gordon and Floquet models, with the advantage of much faster simulations. The main difference is about the precise position of the peaks and their intensity, with Floquet predicting a maximum photocurrent of about one third of the QuantumATK one. For small photon energy (< 0.5 eV), the photocurrent difference could be also due to absorption of photons by gold atoms in the source anchoring group, which increases the number of available electrons for transmission.

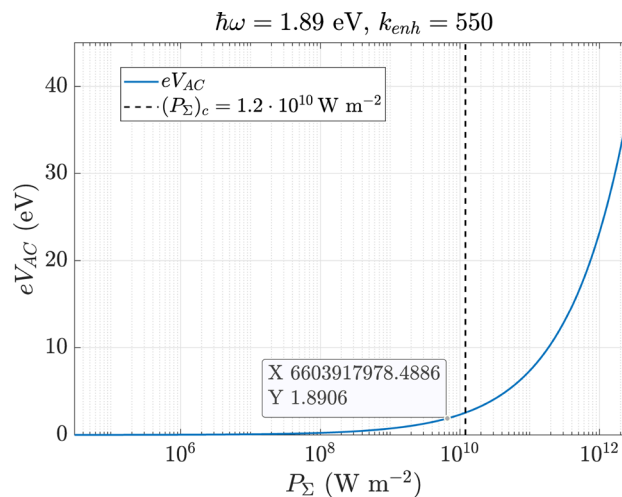


Fig. 7 The blue line corresponds to the relation between the incident power density P_{Σ} and the optical parameter eV_{AC} , whereas the black line is the critical power density $(P_{\Sigma})_c$

On the other hand, for photon energy greater than the HOMO-LUMO gap, the model is no longer valid since we considered only the case of adiabatic interaction of an incident electric field with the molecular junction. In the range of validity, Floquet performs better than Tien-Gordon and in general can be considered a good approximation of QuantumATK for photon energies in the range between 0.5 eV and 1.3 eV

4.2 Experimental validation

The next step was to verify if our simulator is able to reproduce experimental results. A suitable work for a comparison is the one by [66], they measured the current of a suspended wire molecular junction (SWMJ), based on a self-assembled monolayers (SAMs) of octane (C_8H_{18}), for the bias range $V_{DS} \in [0, 1.5]$ V when it is illuminated by a laser. To make a comparison, we had to include the octane molecule in the EE-BESD library. The geometry of the molecule has been optimized with ORCA [68, 69] software using the hybrid DFT functional CAM-B3LYP and the basis set def2-TZVPP [70], including Grimme-D3 dispersion correction in the calculation [71, 72]. The optimized geometry leads to gap length $d_{gap} = 1.541$ nm, which has been used to compute V_{AC} . It is worth underlining that we compared the simulations of a single-molecule junction with the characteristic measurements of a SAM junction, therefore, some effects due to intermolecular interactions could be not taken into account by our simulator.

Regarding the parameters of the incident radiation, the authors in [66] used a laser with wavelength $\lambda = 658$ nm ($E_{ph} = 1.89$ eV) and power density $P_{\Sigma} \approx 6.5 \text{ mWmm}^{-2} = 6.5e9 \text{ Wm}^{-2}$, which result in a surface plasmon amplification $k_{enh} \approx 550$ (estimated by the group). Figure 7 depicts the

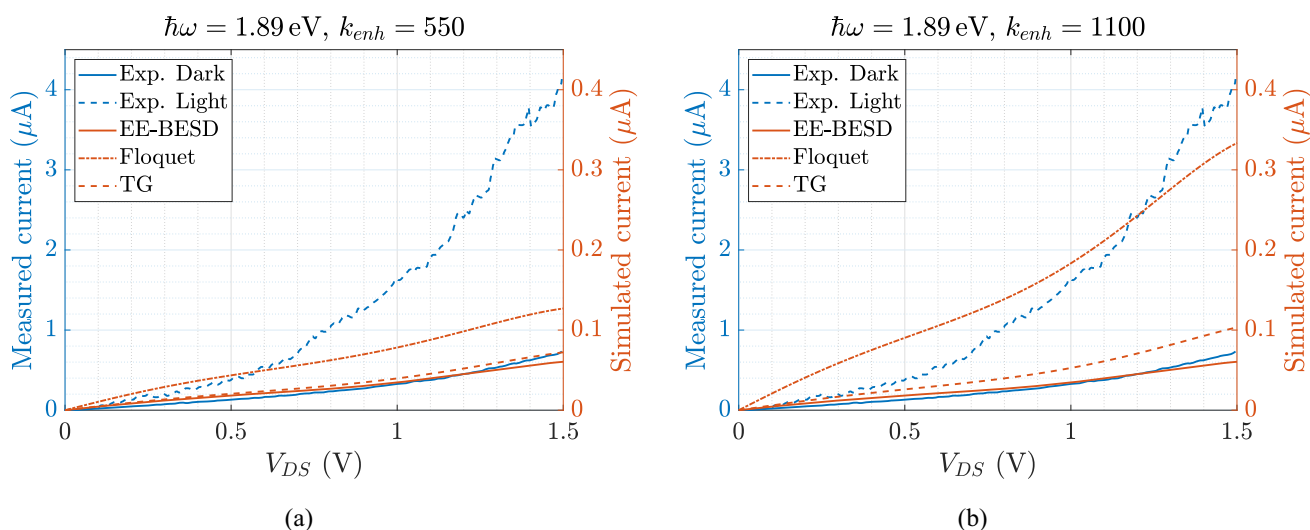


Fig. 8 Experimental validation of EE-BESD-PAT. In (a) and (b) solid and dashed blue lines correspond to the current measured by Arielly et al. in dark and illumination conditions, respectively; the orange solid line is the dark current evaluated by EE-BESD, whereas dash-dotted

and dashed orange lines correspondingly refer to the current calculated in illumination condition by Floquet and Tien-Gordon model. In (a) the enhancement factor is $k_{enh} = 550$ (the same as the considered experiment), while in (b) we consider an enhancement $k_{enh} = 1100$

relation between the incident power density and the value of eV_{AC} considering the parameters of the experiment. The incident power (approximately identified by the data tip) is lower than the critical power density $(P_{\Sigma})_c = 1.2e10 \text{ Wm}^{-2}$ needed to ionize air (the medium through which the radiation propagates), which is crucial otherwise the measured current would have been distorted by the air ionization.

The resulting Floquet and Tien-Gordon parameter, $eV_{AC} \approx 1.87 \text{ eV}$, has been used to simulate the characteristic of the SAM in illumination conditions. The measurements and the results of the simulation with the parameters of the experiment are shown in Fig. 8(a). Starting from the dark current, the EE-BESD prediction is one order of magnitude smaller than the experimental dark current, which is coherent with the fact that in a SAM junction there are more molecules contributing to the current. Regarding the dependence on V_{DS} , the behavior of the two curves is similar, with the experimental one being more exponential-like.

When light is switched on, the measured current increases because the radiation absorption by the molecular junction opens additional channels for electron transmission through the illuminated device (i.e., the light generates subbands presented in Fig. 3). TG predicts a slightly enhanced current but too small w.r.t. experimental one. Actually, it predicts a current under illumination very similar to dark conditions. Therefore, from our results, the TG model, even if simple and computationally extremely efficient, it is not at all able to catch all the physical phenomena involved in PAT through molecular junctions. We believe this to be related to the fact that the TG model implicitly assumes that electrode electron

states are modified by incident light while no significant modification occurs in the unvaried molecular channel. This is not true in general in molecular junctions, where even small modifications of the molecular channel states reflect in significant transport modifications. Indeed, in all mesoscopic systems, the portion of the device mainly affecting the transport is the one with the lowest number of electron states [29], i.e., the molecular channel, while the contacts affect the transport mainly through the channel-contact state mixing. The Floquet model, instead, accurately predicts the experimental data in the range [0, 0.65] V, where it correctly predicts the dark current enhancement produced by the incident radiation. Notice that the absolute value is still a submultiple of the experimental value, and we again relate this to the fact that the considered experiment is performed on a SAM, while our results are related to a single-molecule junction. For V_{DS} greater than 0.65 V also the Floquet model is not capable of predicting the sharp experimental increasing trend of the current under illumination.

To understand the origin of this discrepancy, we decided to test the TG and Floquet models with a larger plasmon enhancing factor, as reported in Fig. 8(b). Indeed, it is not said that the simulated system and the experimental one present the same surface plasmon enhancement factor for the incident radiation wavelength. As already mentioned in this section, k_{enh} could be used as a fitting parameter. We supposed to have an amplification twice the experimental one, i.e., $k_{enh} = 1100$, and repeated the simulation with the resulting induced oscillating potential $eV_{AC} = 3.75 \text{ eV}$. The current amplification predicted by the Floquet model is now comparable with the

experimental one, even though the shape of the curve is not exponential-like as in the experiment since it reflects the shape of EE-BESD dark current. We thus conclude that the Floquet model correctly predicts the shape of the experimental current with $k_{enh} = 550$ for low bias, up to 0.65 V, and the model can be considered validated for small bias values (i.e., in the so-called linear regime of operation). Instead, for larger bias, the model cannot be fairly compared with the experiment since voltage values of 1 V are already sufficient, considering the small dimension of the channel, to modify the conformation shape of the molecule and also affect the stability of the single-molecule junction that might break. The mechanical deformation results in orbitals rearrangement and nonlinear phenomena, which could be completely different from a SAM to a single-molecule junction. Indeed, the field-induced conformational geometrical changes of the molecules inside the SAMs could be much different with respect to the response to such fields for a single molecular junction. We suppose such exponential growth of the experimental current to be related to nonlinear generation phenomena of current carriers, like avalanches or related phenomena (presenting exponential trends) that are not included in the Floquet picture.

The considered experimental work highlights the limits of the TG model, which results intrinsically incapable of catching the main physical phenomena of interest both at small and large bias. The considered experiments validate the EE-BESD-PAT implementation with the Floquet model for moderate applied bias in the regime of a low electric field.

5 Conclusions

We presented an overview of the most common models (Tien-Gordon and Floquet) used to describe the interaction of light with single-molecule junctions in nonequilibrium conditions. We implemented these models through a computationally efficient algorithm, named EE-BESD-PAT, based on NEGF formal framework. The reliability of the algorithm has been tested through comparisons with NEGF-SCBA simulations and experimental measurements. From our results, the TG model appears not reliable for both low and high electric fields, whereas the Floquet model is capable to produce reasonable results in the regime of a low electric field, without losing physical information that we can extract from the transmission spectrum. Furthermore, EE-BESD-PAT results are extremely advantageous in terms of execution time, which is reduced from days to minutes w.r.t. ab initio calculations.

Thanks to EE-BESD-PAT computational efficiency, in the future works, we will focus on its inclusion in photonic circuit-level simulators, thus opening the way to single-molecule optoelectronic devices and circuits. In order to

do so, it will be crucial to have a more precise estimation of the induced voltage V_{AC} and of the plasmonic field amplification factor k_{enh} . Therefore, we will investigate electromagnetic simulations, such as the finite difference time domain (FDTD), required to have a better knowledge of the distribution of the incident field and of possible plasmonic field amplifications, which are strongly dependent on the geometry of the junction.

Author Contributions All the authors conceived the research; AB performed the research tasks and wrote most of the article; FM, CES and YA revised the paper; FM, CES, YA, MG and GP supervised and managed the research schedule and the article writing.

Funding Open access funding provided by Istituto Nazionale di Ricerca Metrologica within the CRUI-CARE Agreement. Open access funding provided by Istituto Nazionale di Ricerca Metrologica (INRiM) within the CRUI-CARE Agreement. The authors have not disclosed any funding.

Data Availability The data that support the findings of this study are available on request from the corresponding author.

Declarations

Conflict of interest The authors declare that there is no conflict of interest.

Open Access This article is licensed under a Creative Commons Attribution 4.0 International License, which permits use, sharing, adaptation, distribution and reproduction in any medium or format, as long as you give appropriate credit to the original author(s) and the source, provide a link to the Creative Commons licence, and indicate if changes were made. The images or other third party material in this article are included in the article's Creative Commons licence, unless indicated otherwise in a credit line to the material. If material is not included in the article's Creative Commons licence and your intended use is not permitted by statutory regulation or exceeds the permitted use, you will need to obtain permission directly from the copyright holder. To view a copy of this licence, visit <http://creativecommons.org/licenses/by/4.0/>.

References

1. Aradhya, S., Venkataraman, L.: Single-molecule junctions beyond electronic transport. *Nature Nanotech* **8**, 399–410 (2013). <https://doi.org/10.1038/nnano.2013.91>
2. Vezzoli, A.: Mechanoresistive single-molecule junctions. *Nanoscale* **14**(8), 2874–2884 (2022)
3. Liang, W., Shores, M., Bockrath, M., Long, J., Park, H.: Kondo resonance in a single-molecule transistor. *Nature* **417**, 725–9 (2002). <https://doi.org/10.1038/nature00790>
4. Zheng, Y., Duan, P., Zhou, Y., Li, C., Zhou, D., Wang, Y., Chen, L.-C., Zhu, Z., Li, X., Bai, J., Qu, K., Gao, T., Shi, J., Liu, J., Zhang, Q.-C., Chen, Z.-N., Hong, W.: Fano resonance in single-molecule junctions. *Angewandte Chemie International Edition* **61**(40), 202210097 (2022). <https://doi.org/10.1002/anie.202210097>
5. Arroyo, C.R., et al.: Signatures of quantum interference effects on charge transport through a single benzene ring. *Angew. Chem. Int. Ed Engl.* **52**(11), 3152–3155 (2013)

6. Vazquez, H., et al.: Probing the conductance superposition law in single-molecule circuits with parallel paths. *Nat. Nanotechnol.* **7**(10), 663–667 (2012)
7. Broman, S.L., Lara-Avila, S., Thisted, C.L., Bond, A.D., Kubatkin, S., Danilov, A., Nielsen, M.B.: Dihydroazulene photoswitch operating in sequential tunneling regime: Synthesis and single-molecule junction studies. *Advanced Functional Materials* **22**(20), 4249–4258 (2012). <https://doi.org/10.1002/adfm.201200897> (<https://onlinelibrary.wiley.com/doi/pdf/10.1002/adfm.201200897>)
8. Gemma, A., Gotsmann, B.: Will molecules ever sit at the thermo-electric table? (2021)
9. Aviram, A., Ratner, M.A.: Molecular rectifiers. *Chemical Physics Letters* **29**(2), 277–283 (1974). [https://doi.org/10.1016/0009-2614\(74\)85031-1](https://doi.org/10.1016/0009-2614(74)85031-1)
10. Li, T., Bandari, V.K., Schmidt, O.G.: Molecular electronics: Creating and bridging molecular junctions and promoting its commercialization. *Adv. Mater.* **35**(22), 2209088 (2023)
11. Wang, K., Meyhofer, E., Reddy, P.: Thermal and thermo-electric properties of molecular junctions. *Advanced Functional Materials* **30**(8), 1904534 (2020). <https://doi.org/10.1002/adfm.201904534> (<https://onlinelibrary.wiley.com/doi/pdf/10.1002/adfm.201904534>)
12. Roldan, D., Kaliginedi, V., Cobo, S., Kolivoska, V., Bucher, C., Hong, W., Royal, G., Wandlowski, T.: Charge transport in photoswitchable dimethyldihydropyrene-type single-molecule junctions. *Journal of the American Chemical Society* **135**(16), 5974–5977 (2013). <https://doi.org/10.1021/ja401484j>. (PMID: **23574365**)
13. Daaoub, A., Sangtarash, S., Sadeghi, H.: Switching quantum interference in phenoxyquinone single molecule junction with light. *Nanomaterials* **10**(8) (2020). <https://doi.org/10.3390/nano10081544>
14. Mo, F., Ardesi, Y., Roch, M.R., Graziano, M., Piccinini, G.: Investigation of amperometric sensing mechanism in gold–c60–gold molecular dot. *IEEE Sensors Journal* **22**(20), 19152–19161 (2022). <https://doi.org/10.1109/JSEN.2022.3203513>
15. Mo, F., Spano, C.E., Ardesi, Y., Roch, M.R., Piccinini, G., Graziano, M.: Single-molecule aflatoxin b1 sensing via pyrrole-based molecular quantum dot. In: 2022 IEEE 22nd International Conference on Nanotechnology (NANO), pp. 153–156 (2022). <https://doi.org/10.1109/NANO54668.2022.9928694>
16. Mo, F., Spano, C.E., Ardesi, Y., Ruo Roch, M., Piccinini, G., Graziano, M.: Design of pyrrole-based gate-controlled molecular junctions optimized for single-molecule aflatoxin b1 detection. *Sensors* **23**(3) (2023). <https://doi.org/10.3390/s23031687>
17. Mo, F., Ardesi, Y., Spano, C.E., Roch, M.R., Piccinini, G., Graziano, M.: Effect of adsorption mechanism on conduction in single-molecule pyrrole-based sensor for afb1. *IEEE Transactions on Nanotechnology* **22**, 811–816 (2023). <https://doi.org/10.1109/TNANO.2023.3336522>
18. Li, J., et al.: Room-temperature logic-in-memory operations in single-metallofullerene devices. *Nat. Mater.* **21**(8), 917–923 (2022)
19. Spano, C.E., Mo, F., Ardesi, Y., Roch, M.R., Piccinini, G., Graziano, M.: Electronic transport study of bistable Cr@C28 single molecule device for high-density data storage applications. In: Proceedings of the 8th World Congress on New Technologies. Avestia Publishing, (2022)
20. Ardesi, Y., Mo, F., Spano, C.E., Ardia, G., Piccinini, G., Graziano, M.: Conformation-based molecular memories for nanoscale mem-computing. In: 2023 IEEE 23rd International Conference on Nanotechnology (NANO), pp. 694–697 (2023). <https://doi.org/10.1109/NANO58406.2023.10231199>
21. Sil, A., Alsaqr, M., Spano, C.E., Larbi, A., Higgins, S.J., Robertson, C.M., Graziano, M., Sangtarash, S., Nichols, R.J., Sadeghi, H., Vezzoli, A.: Mechanical manipulation of quantum interference in single-molecule junctions. *Small* **20**(25), 2308865 (2024). <https://doi.org/10.1002/smll.202308865> (<https://onlinelibrary.wiley.com/doi/pdf/10.1002/smll.202308865>)
22. Sil, A., Spano, C.E., Chelli, Y., Higgins, S., Sangtarash, S., Piccinini, G., Graziano, M., Nichols, R., Hatfe, S., Vezzoli, A.: Single-molecule mechanoresistivity by intermetallic bonding. *ChemRxiv* (2024) <https://doi.org/10.26434/chemrxiv-2024-x1rr1>
23. Meng, L., et al.: Dual-gated single-molecule field-effect transistors beyond moore’s law. *Nature Communications* **13**, 1410 (2022) <https://doi.org/10.1038/s41467-022-28999-x>
24. Wu, C., Qiao, X., Robertson, C.M., Higgins, S.J., Cai, C., Nichols, R.J., Vezzoli, A.: A chemically soldered polyoxometalate single-molecule transistor. *Angewandte Chemie International Edition* **59**(29), 12029–12034 (2020). <https://doi.org/10.1002/anie.202002174>. (<https://onlinelibrary.wiley.com/doi/pdf/10.1002/anie.202002174>)
25. Spano, C.E., Ardesi, Y., Piccinini, G., Graziano, M.: Enhancing the on/off current ratio in single-molecule FET via destructive quantum interference. *IEEE Trans. Electron Devices* **69**(10), 5906–5912 (2022)
26. Taylor, J., Guo, H., Wang, J.: Ab initio modeling of quantum transport properties of molecular electronic devices. *Phys. Rev. B* **63**, 245407 (2001). <https://doi.org/10.1103/PhysRevB.63.245407>
27. Brandbyge, M., Mozos, J.-L., Ordejón, P., Taylor, J., Stokbro, K.: Density-functional method for nonequilibrium electron transport. *Phys. Rev. B* **65**, 165401 (2002). <https://doi.org/10.1103/PhysRevB.65.165401>
28. Zahid, F., Paulsson, M., Polizzi, E., Ghosh, A.W., Siddiqui, L., Datta, S.: A self-consistent transport model for molecular conduction based on extended hückel theory with full three-dimensional electrostatics. *The Journal of Chemical Physics* **123**(6), 064707 (2005). <https://doi.org/10.1063/1.1961289>
29. Datta, S.: *Quantum Transport: Atom to Transistor*. Cambridge University Press, Cambridge (2005)
30. Synopsys: QuantumATK S-2021.06 Documentation. (2021). Synopsys. <https://docs.quantumatk.com/manual/manual.html>
31. Zahir, A., et al.: Ee-besd: molecular fet modeling for efficient and effective nanocomputing design. *Journal of Computational Electronics* **15**, 479–491 (2016). <https://doi.org/10.1007/s10825-015-0777-y>
32. Galperin, M., Nitzan, A.: Molecular optoelectronics: the interaction of molecular conduction junctions with light. *Phys. Chem. Chem. Phys.* **14**, 9421–9438 (2012). <https://doi.org/10.1039/C2CP40636E>
33. Wang, T., Nijhuis, C.A.: Molecular electronic plasmonics. *Applied Materials Today* **3**, 73–86 (2016). <https://doi.org/10.1016/j.apmt.2016.03.001>
34. Chen, L., Feng, A., Wang, M., et al.: Towards single-molecule optoelectronic devices. *Sci. China Chem.* **61**, 1368–1384 (2018). <https://doi.org/10.1007/s11426-018-9356-2>
35. Lacroix, J.-C., et al.: From active plasmonic devices to plasmonic molecular electronics. *Polymer International* **68**(4), 607–619 (2019). <https://doi.org/10.1002/pi.5756>
36. Kos, D., Assumpcao, D.R., Guo, C., Baumberg, J.J.: Quantum tunneling induced optical rectification and plasmon-enhanced photocurrent in nanocavity molecular junctions. *ACS Nano* **15**(9), 14535–14543 (2021). <https://doi.org/10.1021/acsnano.1c04100>
37. Noy, G., Ophir, A., Selzer, Y.: Response of molecular junctions to surface plasmon polaritons. *Angewandte Chemie International Edition* **49**(33), 5734–5736 (2010). <https://doi.org/10.1002/anie.201000972>
38. Vadai, M., et al.: Plasmon-induced conductance enhancement in single-molecule junctions. *The Journal of Physical Chemistry Letters* **4**(17), 2811–2816 (2013). <https://doi.org/10.1021/jz4014008>

39. Fung, E., et al.: Too hot for photon-assisted transport: Hot-electrons dominate conductance enhancement in illuminated single-molecule junctions. *Nano Letters* **17**(2), 1255–1261 (2017). <https://doi.org/10.1021/acs.nanolett.6b05091>
40. Brongersma, M., Halas, N., Nordlander, P.: Plasmon-induced hot carrier science and technology. *Nature Nanotech* **10**, 25–34 (2015). <https://doi.org/10.1038/nnano.2014.311>
41. Selzer, Y.: Elucidating the contributions of plasmon-induced excitons and hot carriers to the photocurrent of molecular junctions. *The Journal of Physical Chemistry C* **124**(16), 8680–8688 (2020). <https://doi.org/10.1021/acs.jpcc.0c02196>
42. Hong, W., Lan, J., Li, H., Yan, Z., Li, Y., Jiang, H., Chen, M.: Towards an understanding of the localized surface plasmon resonance decay pathways in bimetallic core-shell nanoparticles. *Optics & Laser Technology* **146**, 107565 (2022). <https://doi.org/10.1016/j.optlastec.2021.107565>
43. Cuevas, J.C., Scheer, E.: *Molecular Electronics: An Introduction to Theory and Experiment*. World Scientific Publishing Co. Pte. Ltd., (2010). Chap. 8, 20, Appendix A
44. Aeberhard, U.: A microscopic theory of quantum well photovoltaics. Ph.D. thesis, ETH, Zürich (2008). <https://www.research-collection.ethz.ch/handle/20.500.11850/150994>
45. Henrickson, L.E.: Nonequilibrium photocurrent modeling in resonant tunneling photodetectors. *Journal of Applied Physics* **91**(10), 6273–6281 (2002). <https://doi.org/10.1063/1.1473677>
46. Chen, J., Hu, Y., Guo, H.: First-principles analysis of photocurrent in graphene *pn* junctions. *Phys. Rev. B* **85**(15), 155441 (2012). <https://doi.org/10.1103/PhysRevB.85.155441>
47. Zhang, L., et al.: Generation and transport of valley-polarized current in transition-metal dichalcogenides. *Phys. Rev. B* **90**(19), 195428 (2014). <https://doi.org/10.1103/PhysRevB.90.195428>
48. Palsgaard, M., Markussen, T., Gunst, T., Brandbyge, M., Stokbro, K.: Efficient first-principles calculation of phonon-assisted photocurrent in large-scale solar-cell devices. *Physical Review Applied* **10**(1), 014026 (2018). <https://doi.org/10.1103/physrevapplied.10.014026>
49. Palsgaard, M., et al.: Stacked janus device concepts: Abrupt *pn*-junctions and cross-plane channels. *Nano Letters* **18**(11), 7275–7281 (2018). <https://doi.org/10.1021/acs.nanolett.8b03474>
50. Tien, P.K., Gordon, J.P.: Multiphoton process observed in the interaction of microwave fields with the tunneling between superconductor films. *Phys. Rev.* **129**(2), 647–651 (1963). <https://doi.org/10.1103/PhysRev.129.647>
51. Pedersen, M.H., Büttiker, M.: Scattering theory of photon-assisted electron transport. *Physical Review B* **58**(19), 12993–13006 (1998). <https://doi.org/10.1103/physrevb.58.12993>
52. Viljas, J.K., Cuevas, J.C.: Role of electronic structure in photoassisted transport through atomic-sized contacts. *Phys. Rev. B* **75**(7) (2007). <https://doi.org/10.1103/physrevb.75.075406>
53. Viljas, J.K., Pauly, F., Cuevas, J.C.: Photoconductance of organic single-molecule contacts. *Phys. Rev. B* **76**(3), 033403 (2007). <https://doi.org/10.1103/PhysRevB.76.033403>
54. Viljas, J.K., Pauly, F., Cuevas, J.C.: Modeling elastic and photoassisted transport in organic molecular wires: Length dependence and current-voltage characteristics. *Phys. Rev. B* **77**(15), 155119 (2008). <https://doi.org/10.1103/PhysRevB.77.155119>
55. Oppenländer, C.: Time-dependent density functional tight binding combined with the liouville-von neumann equation applied to ac transport in molecular electronics. PhD thesis, Universität Regensburg, Regensburg (Oct 2014). https://epub.uni-regensburg.de/31257/1/Dissertation_Oppenlender.pdf
56. Tikhonov, A., Coalson, R.D., Dahnovsky, Y.: Calculating electron transport in a tight binding model of a field-driven molecular wire: Floquet theory approach. *The Journal of Chemical Physics* **116**(24), 10909–10920 (2002). <https://doi.org/10.1063/1.1448292>
57. Kohler, S., Lehmann, J., Hänggi, P.: Controlling currents through molecular wires. *Superlattices and Microstructures* **34**(3), 419–427 (2003). <https://doi.org/10.1016/j.spmi.2004.03.038>
58. Kohler, S., Lehmann, J., Hänggi, P.: Driven quantum transport on the nanoscale. *Physics Reports* **406**(6), 379–443 (2005). <https://doi.org/10.1016/j.physrep.2004.11.002>
59. Martinez, D.F.: Floquet–green function formalism for harmonically driven hamiltonians. *Journal of Physics A: Mathematical and General* **36**(38), 9827–9842 (2003). <https://doi.org/10.1088/0305-4470/36/38/302>
60. Stefanucci, G., Kurth, S., Rubio, A., Gross, E.K.U.: Time-dependent approach to electron pumping in open quantum systems. *Phys. Rev. B* **77**(7), 075339 (2008). <https://doi.org/10.1103/PhysRevB.77.075339>
61. Hsu, L.-Y., Xie, D., Rabitz, H.: Light-driven electron transport through a molecular junction based on cross-conjugated systems. *The Journal of Chemical Physics* **141**(12), 124703 (2014). <https://doi.org/10.1063/1.4895963>
62. Hsu, L.-Y., Rabitz, H.: Coherent light-driven electron transport through polycyclic aromatic hydrocarbon: laser frequency, field intensity, and polarization angle dependence. *Phys. Chem. Chem. Phys.* **17**, 20617–20629 (2015). <https://doi.org/10.1039/C5CP02663F>
63. Genske, M.: Periodically driven many-body quantum systems. quantum ratchets, topological states and the floquet-boltzmann equation. PhD thesis, Univ. of Cologne, Köln (Jul 2017). https://kups.uni-koeln.de/7822/1/thesis_final_A4.pdf
64. Gu, B., Franco, I.: Optical absorption properties of laser-driven matter. *Phys. Rev. A* **98**(6), 063412 (2018). <https://doi.org/10.1103/PhysRevA.98.063412>
65. Cabra, G., Franco, I., Galperin, M.: Optical properties of periodically driven open nonequilibrium quantum systems. *The Journal of Chemical Physics* **152**(9), 094101 (2020). <https://doi.org/10.1063/1.5144779>
66. Arielly, R., Ofarim, A., Noy, G., Selzer, Y.: Accurate determination of plasmonic fields in molecular junctions by current rectification at optical frequencies. *Nano Letters* **11**(7), 2968–2972 (2011). <https://doi.org/10.1021/nl201517k>
67. Amendola, V., Pilot, R., Frascioni, M., Maragò, O.M., Iatì, M.A.: Surface plasmon resonance in gold nanoparticles: a review. *Journal of Physics: Condensed Matter* **29**(20), 203002 (2017). <https://doi.org/10.1088/1361-648x/aa60f3>
68. Neese, F.: The orca program system. *WIREs Computational Molecular Science* **2**(1), 73–78 (2012). <https://doi.org/10.1002/wcms.81>
69. Neese, F.: Software update: the orca program system, version 4.0. *WIREs Computational Molecular Science* **8**(1), 1327 (2018). <https://doi.org/10.1002/wcms.1327>
70. Weigend, F., Ahlrichs, R.: Balanced basis sets of split valence, triple zeta valence and quadruple zeta valence quality for h to rn: Design and assessment of accuracy. *Phys. Chem. Chem. Phys.* **7**, 3297–3305 (2005). <https://doi.org/10.1039/B508541A>
71. Grimme, S., Antony, J., Ehrlich, S., Krieg, H.: A consistent and accurate ab initio parametrization of density functional dispersion correction (dft-d) for the 94 elements h-pu. *The Journal of Chemical Physics* **132**(15), 154104 (2010). <https://doi.org/10.1063/1.3382344>
72. Grimme, S., Ehrlich, S., Goerigk, L.: Effect of the damping function in dispersion corrected density functional theory. *Journal of Computational Chemistry* **32**(7), 1456–1465 (2011). <https://doi.org/10.1002/jcc.21759>